AFRL-RX-WP-JA-2015-0131

INFLUENCE OF INTERFACIAL CARBIDE LAYER CHARACTERISTICS ON THERMAL PROPERTIES OF COPPER-DIAMOND COMPOSITES (POSTPRINT)

J.E. Spowart
AFRL/RXCM

V. Sinha
UES, Inc.

APRIL 2014
Interim Report

Distribution Statement A. Approved for public release; distribution unlimited.

See additional restrictions described on inside pages

STINFO COPY

© Springer Science+Business Media, LLC 2012

AIR FORCE RESEARCH LABORATORY
MATERIALS AND MANUFACTURING DIRECTORATE
WRIGHT-PATTERSON AIR FORCE BASE OH 45433-7750
AIR FORCE MATERIEL COMMAND
UNITED STATES AIR FORCE

NOTICE AND SIGNATURE PAGE

Using Government drawings, specifications, or other data included in this document for any purpose other than Government procurement does not in any way obligate the U.S. Government. The fact that the Government formulated or supplied the drawings, specifications, or other data does not license the holder or any other person or corporation; or convey any rights or permission to manufacture, use, or sell any patented invention that may relate to them.

Qualified requestors may obtain copies of this report from the Defense Technical Information Center (DTIC) (http://www.dtic.mil).

AFRL-RX-WP-JA-2015-0131 HAS BEEN REVIEWED AND IS APPROVED FOR PUBLICATION IN ACCORDANCE WITH ASSIGNED DISTRIBUTION STATEMENT.

//Signature//

MICHEAL E. BURBA, Project Engineer
Metals Branch
Structural Materials Division

//Signature//

DANIEL J. EVANS, Chief
Metals Branch
Structural Materials Division

//Signature//

ROBERT T. MARSHALL, Deputy Chief
Structural Materials Division
Materials And Manufacturing Directorate

This report is published in the interest of scientific and technical information exchange and its publication does not constitute the Government's approval or disapproval of its ideas or findings.

REPORT DOCUMENTATION PAGE

Form Approved
OMB No. 0704-0188

The public reporting burden for this collection of information is estimated to average 1 hour per response, including the time for reviewing instructions, searching existing data sources, gathering and maintaining the data needed, and completing and reviewing the collection of information. Send comments regarding this burden estimate or any other aspect of this collection of information, including suggestions for reducing this burden, to Department of Defense, Washington Headquarters Services, Directorate for Information Operations and Reports (0704-0188), 1215 Jefferson Davis Highway, Suite 1204, Arlington, VA 22202-4302. Respondents should be aware that notwithstanding any other provision of law, no person shall be subject to any penalty for failing to comply with a collection of information if it does not display a currently valid OMB control number. **PLEASE DO NOT RETURN YOUR FORM TO THE ABOVE ADDRESS**.

1. REPORT DATE *(DD-MM-YY)*	2. REPORT TYPE	3. DATES COVERED *(From - To)*
April 2014	Interim	19 March 2014 – 31 March 2014

4. TITLE AND SUBTITLE
INFLUENCE OF INTERFACIAL CARBIDE LAYER CHARACTERISTICS ON THERMAL PROPERTIES OF COPPER-DIAMOND COMPOSITES (POSTPRINT)

5a. CONTRACT NUMBER
In-house

5b. GRANT NUMBER

5c. PROGRAM ELEMENT NUMBER
62102F

6. AUTHOR(S)
J.E. Spowart - AFRL/RXCM
V. Sinha – UES, Inc.

5d. PROJECT NUMBER
4349

5e. TASK NUMBER

5f. WORK UNIT NUMBER
X0W6

7. PERFORMING ORGANIZATION NAME(S) AND ADDRESS(ES)

AFRL/RXCM
2941 Hobson Way
Bldg 654, Rm 136
Wright-Patterson AFB, OH 45433

UES, Inc.
4401 Dayton-Xenia Rd.
Dayton, OH 45432-1894

8. PERFORMING ORGANIZATION REPORT NUMBER

9. SPONSORING/MONITORING AGENCY NAME(S) AND ADDRESS(ES)

Air Force Research Laboratory
Materials and Manufacturing Directorate
Wright-Patterson Air Force Base, OH 45433-7750
Air Force Materiel Command
United States Air Force

10. SPONSORING/MONITORING AGENCY ACRONYM(S)
AFRL/RXCM

11. SPONSORING/MONITORING AGENCY REPORT NUMBER(S)
AFRL-RX-WP-JA-2015-0131

12. DISTRIBUTION/AVAILABILITY STATEMENT
Distribution Statement A. Approved for public release; distribution unlimited.

13. SUPPLEMENTARY NOTES
Journal article published in *J Mater Sci* (2013) 48: 1330-1341. © Springer Science+Business Media, LLC 2012. The U.S. Government is joint author of the work and has the right to use, modify, reproduce, release, perform, display or disclose the work. This report contains color. The final publication is available at DOI 10.1007/s10853-012-6878-0.

14. ABSTRACT

Copper–diamond composites are increasingly being considered for thermal management applications because of their attractive combination of properties, such as high thermal conductivity (λ) and low coefficient of thermal expansion (CTE). In this research, thermal properties of Cu–diamond composites with two different types of interfacial carbides (Cr_3C_2 and SiC) were studied. The interface thermal conductance (h_c) was calculated with Maxwell mean-field and differential effective medium schemes, wherein experimentally measured λ was entered as an input parameter. The λ and h_c of both the Cu–Cr_3C_2–diamond and Cu–SiC–diamond composites are higher than those reported in previous studies for Cu–diamond composites with no interfacial carbides. The value of h_c is intimately related to the morphology and thickness of the interface carbide layer, with the highest h_c being associated with a thin and continuous interface carbide layer. A lower h_c resulting from a thicker Cr_3C_2 layer can provide an alternate explanation for a previously reported trend in λ of Cu–Cr_3C_2–diamond composites with different Cr-contents. The experimentally measured CTE was compared with the Turner and Kerner model predictions. The CTE of both the Cu–Cr_3C_2–diamond and Cu–SiC–diamond composites is lower and better matches the model predictions than the previously reported CTE of Cu–diamond composite with no interfacial carbides. The CTE of Cu–Cr_3C_2–diamond composites agrees better with the Kerner model than the Turner model, which suggests that deformation during temperature excursions involves shear.

15. SUBJECT TERMS
thermal management, copper-diamond substrates, low coefficient of thermal expansion

16. SECURITY CLASSIFICATION OF:			17. LIMITATION OF ABSTRACT:	18. NUMBER OF PAGES	19a. NAME OF RESPONSIBLE PERSON (Monitor)
a. REPORT	b. ABSTRACT	c. THIS PAGE			Micheal E. Burba
Unclassified	Unclassified	Unclassified	SAR	15	19b. TELEPHONE NUMBER *(Include Area Code)* (937) 255-9795

J Mater Sci (2013) 48:1330 1341
DOI 10.1007/s10853 012 6878 0

Influence of interfacial carbide layer characteristics on thermal properties of copper–diamond composites

V. Sinha · J. E. Spowart

Received: 2 July 2012 / Accepted: 6 September 2012 / Published online: 28 September 2012
© Springer Science+Business Media, LLC 2012

Abstract Copper diamond composites are increasingly being considered for thermal management applications because of their attractive combination of properties, such as high thermal conductivity (λ) and low coefficient of thermal expansion (CTE). In this research, thermal properties of Cu diamond composites with two different types of interfacial carbides (Cr_3C_2 and SiC) were studied. The interface thermal conductance (h_c) was calculated with Maxwell mean-field and differential effective medium schemes, wherein experimentally measured λ was entered as an input parameter. The λ and h_c of both the Cu Cr_3C_2 diamond and Cu SiC diamond composites are higher than those reported in previous studies for Cu diamond composites with no interfacial carbides. The value of h_c is intimately related to the morphology and thickness of the interface carbide layer, with the highest h_c being associated with a thin and continuous interface carbide layer. A lower h_c resulting from a thicker Cr_3C_2 layer can provide an alternate explanation for a previously reported trend in λ of Cu Cr_3C_2 diamond composites with different Cr-contents. The experimentally measured CTE was compared with the Turner and Kerner model predictions. The CTE of both the Cu Cr_3C_2 diamond and Cu SiC diamond composites is lower and better matches the model predictions than the previously reported CTE of Cu diamond composite with no interfacial carbides. The CTE of Cu Cr_3C_2 diamond composites agrees better with the Kerner model than the Turner model, which suggests that deformation during temperature excursions involves shear.

V. Sinha (✉) · J. E. Spowart
Air Force Research Laboratory, Materials and Manufacturing Directorate, Wright Patterson Air Force Base, OH 45433, USA
e mail: vikas.sinha@wpafb.af.mil

V. Sinha
UES, Inc., 4401 Dayton Xenia Road, Dayton, OH 45432, USA

Introduction

A reliable operation as well as further improvements in performance of advanced electronic components requires a creditable thermal management strategy. A high thermal conductivity and a tailorable coefficient of thermal expansion (CTE) are important attributes of candidate substrate/packaging materials for high power density electronic components [1 6]. Several diamond containing metal matrix composites have been developed to generate this combination of properties and in many instances, these are materials of choice for such thermal management applications.

In several metal diamond systems, carbides at the interface improve the integrity, adhesion (via mechanical and/or chemical bonding), and aid the thermal transport between metal and diamond [2 6]. A variety of carbides are known to serve this purpose, e.g., Cr carbide in Cu- and Ag-matrix composites, B carbide in Cu-matrix composite, SiC in Ag-matrix composite, etc. In addition, carbides at diamond/metal interface also improve the wettability during liquid metal infiltration of diamond and therefore, carbide-forming elements are added to liquid metal prior to infiltration for this purpose as well [2, 3]. In cases where these carbide-forming elements undergo a eutectic reaction with the matrix metal, the infiltration temperature can be reduced and thereby, graphitization of diamond at the interface can be minimized [2]. This further aids the processing and leads to better thermal properties. Examples include Cu B, Cu Cr, Ag Cr and Ag Si systems.

Besides liquid phase infiltration, the composites can be fabricated via powder metallurgy route by sintering in the

Distribution Statement A. Approved for public release; distribution unlimited.

solid state [4 6]. In prior studies (e.g., Ref. [6]), a mixture of pre-alloyed Cu Cr powder and diamond particles was hot pressed to fabricate composites with good thermal properties. Prior investigations have reported a change in composite thermal conductivity (λ) and Cu/diamond interface thermal conductance (h_c) with a change in material or processing conditions [3, 6]. However, the underlying microstructural features leading to these observed differences in h_c and λ are not fully understood. The objective of this study is to identify the microstructural features that cause the variations in h_c, and thereby the differences in λ.

For fabrication via powder metallurgy route, the processing temperatures are much lower and additionally, liquid metal wettability of diamond is not an issue. Moreover, the solid-state processing can, in principle, be carried out at relatively low temperatures even for non-eutectic matrices. For example, although Cu Si is not a eutectic system, a Cu diamond composite with a SiC interface layer can be fabricated at a relatively low temperature via solid-state processing route.

The CTE of SiC is comparable to that of B carbide and about half of Cr carbide (Table 1). Moreover, there is a large variation in the reported values of thermal conductivity for SiC; with the minimum being similar to that for Cr_3C_2 and B_4C, and the maximum being more than an order of magnitude higher (Table 1). Therefore, it is reasonable to expect that use of SiC in lieu of B carbide or Cr carbide as an interface layer can potentially lead to a similar or higher λ. In an earlier work [13], fabrication of a Cu diamond composite with a SiC interface layer was attempted. The λ of this composite was very low ($\sim$60 W/m-K). The current paper also assesses if an improvement in λ of a Cu diamond composite with a SiC interface layer can be effected by process modification.

The thermal properties of Cu SiC metal matrix composites, which *do not* contain diamond, have been examined in prior studies with an aim to evaluate their suitability as a thermal management material [6, 14 16]. There is an issue with regards to a chemical reaction between Cu and SiC at elevated temperatures, which results in decomposition of SiC and dissolution of Si in Cu-matrix. Thermal conductivity of Cu is reduced significantly due to this reaction, especially when processing temperatures are above the melting point of Cu [14, 15]. Moreover, when solid-state processing of Cu SiC composite involves relatively *long* thermal exposures, its thermal properties are adversely affected [6, 16]. However, it has been shown that this reaction can be minimized, and its adverse effect on thermal conductivity can essentially be eliminated via solid-state processing (forging) that incorporates a *short* thermal exposure [14, 16].

In this study, thermal properties of Cu diamond composites with two different types of interfacial carbides (i.e., Cr_3C_2 and SiC) were investigated. To fabricate the Cu Cr_3C_2 diamond composites, a mixture of pre-alloyed Cu Cr powder and diamond particles was hot pressed for sufficient time at a high enough temperature to allow diffusion of Cr-atoms to the metal/diamond interface with the resultant formation of carbide. On the other hand, to fabricate the Cu SiC diamond composite, Cu SiC diamond powder was forged for short time at a relatively low temperature to minimize the diffusion of Si away from interface into the Cu-matrix.

Table 1 Thermal properties of carbides [7 12]

Type of carbide	CTE ($\times 10^{-6}$/K)	Thermal conductivity (W/m K)	References
SiC	3.8 5.1	40 145	[7, 8]
SiC		300 500	[9 11]
Cr_3C_2	10.4	19	[12]
B_4C	4.3	20 35	[7]

Material

Composites with Cr carbide interface layer

Composites with three different amounts of diamond (20, 40, and 60 vol%) were examined. The diamond particle size was $-120/+140$ mesh (average $\sim$110 μm) for 20 and 40 vol% diamond composites. For 60 vol% diamond composite, a mixture of diamond particle sizes was used that consisted of $\sim$75 % of $-70/+80$ mesh (average $\sim$194 μm) and $\sim$25 % of $-325/+400$ mesh (average $\sim$40 μm). The pre-alloyed Cu Cr powder, with nominal composition of Cu 0.8 wt%Cr, was used to form Cu-rich matrix in the composites. The composites were fabricated via hot pressing in a vacuum of $\sim 10^{-4}$ mbar ($\sim 10^{-2}$ Pa). The hot pressing was done by Fraunhofer Institute (IFAM, Dresden, Germany) at a pressure of 45 MPa and a temperature of 950 °C, with the hold time of 30 min. The material and processing conditions are summarized in Table 2, where the composites with 20, 40 and 60 vol% diamond are designated 'A', 'B', and 'C', respectively. The microstructures of the three composites are shown in Fig. 1a c.

Composites with Si carbide interface layer

Diamond particles (average size $\sim$110 μm) were coated with SiC using a proprietary chemical vapor reaction process [17]. To reduce any possible segregation of diamond in the composite, SiC-coated diamond particles were further plated with Cu (using a commercial electro-plating

Distribution Statement A. Approved for public release; distribution unlimited.

technique) and no additional Cu powder was added prior to consolidation. The Cu SiC diamond powder had an average particle size of ~160 μm. The approach in this study for reducing diamond segregation in Cu SiC diamond composite is consistent with the earlier reports [16, 18].

These two-step coated diamond particles were subsequently consolidated via forging in an inert atmosphere. The forging was done by AM^{2}T, LLC (formerly Ceracon, Inc., Sacramento, CA) at a pressure of 345 MPa and a temperature of 850 °C (the forging time was ~10 s). The consolidated composite was subsequently air-cooled to room temperature. The material and processing conditions are summarized in Table 2, where the Cu SiC diamond composite is designated 'D'. The microstructure of composite D is shown in Fig. 1d.

Experimental procedures

Determination of thermal properties

The λ of the four composites was calculated as: $\lambda = \rho.D.c_p$, where ρ is the density, D is the thermal diffusivity, and c_p is the specific heat capacity. ρ was measured using Archimedes' method, and D was measured with laser flash technique per ASTM E1461. The specimens for D measurement (nominal dimensions: 10 mm × 10 mm × 3 mm) were coated with ~5 μm of graphite prior to loading in a sample holder in LFA 457 MicroFlash unit (Manufacturer: NETZSCH-Gerätebau GmbH, Selb, Germany) between a neodymium glass laser (wavelength = 1.06 μm and pulse width = 330 μs) and an indium antimonide (InSb) infrared (IR) detector. The graphite coating is used to improve absorption of laser pulse energy on the front face, and to improve emissivity of the rear face of specimen. The specimen is subjected to a short duration laser pulse. The energy of pulse is absorbed by the front face of specimen and the resulting rear face temperature rise with time is recorded using the IR detector. The temperature rise curve is analyzed with NETZSCH LFA Analysis software, wherein different models (including combinations of facial and radial heat loss, and finite pulse effect) can be selected. The analysis is based on nonlinear regression routines, which consider the entire measurement curve (about 2000 3000 data points) by adjusting the unknown diffusivity and loss factor until the total point-to-point mismatch between the theoretical and experimental temperature rise curves is minimized. The measurement and analysis were validated in the software by visual and statistical comparisons of the model and experimental temperature rise curves. c_p was calculated from rule-of-mixtures (ROM) using c_p of Cu $(c_{p_{Cu}}) =$ 385 J/kg-K [19] and c_p of diamond $(c_{p_{Diamond}}) = 510$ J/kg-K [20]. The composite c_p using ROM is obtained as: $c_{p_{Composite}} = W_{Cu} \times c_{p_{Cu}} + W_{Diamond} \times c_{p_{Diamond}}$, where W_{Cu} and $W_{Diamond}$ are the weight fractions of Cu and diamond, respectively. The CTE of composites was measured with a push-rod dilatometer DIL 402 C (Manufacturer: NETZSCH-Gerätebau GmbH, Selb, Germany) per ASTM E228 at a heating rate of 1 °C/min in nitrogen atmosphere. The reported values of CTE were determined for the temperature range 25 100 °C, using the Technical Alpha Values Routine in the Proteus Analysis software from NETZSCH.

Characterization of interfacial carbides

To detect the presence of any carbide at the Cu/diamond interface and to determine its salient features, the composites were immersed in dilute nitric acid to dissolve the copper matrix. The diamond particles, along with the interfacial carbides, were collected and subsequently characterized via scanning electron microscopy (SEM), X-ray diffraction (XRD), and electron probe microanalysis (EPMA). SEM, XRD, and EPMA examinations were carried out to characterize

Table 2 Summary of materials and processing conditions of the examined composites

Composite[a]	Amount of diamond (vol%)	Average diamond particle diameter (μm)	Pre consolidation processing	Consolidation method	Consolidation parameters		
					Pressure (MPa)	Temperature (°C)	Hold time
A	20	110	Synthetic diamond particles mixed with pre alloyed Cu 0.8 wt%Cr powder	Hot pressing	45	950	30 min
B	40	110					
C	60	156[b]					
D	34	110	Synthetic diamond particles first coated with SiC, and then plated with Cu	Forging	345	850	~10 s

[a] Composites A, B and C were supplied by Dr. Thomas Schubert (IFAM, Dresden, Germany), whereas composite D was provided by Mr. Henry "Mic" Meeks of AM^{2}T, LLC (formerly Ceracon, Inc.)

[b] Weighted average of bi modal particle size distribution: 194 μm (~75 %) and 40 μm (~25 %)

Distribution Statement A. Approved for public release; distribution unlimited.

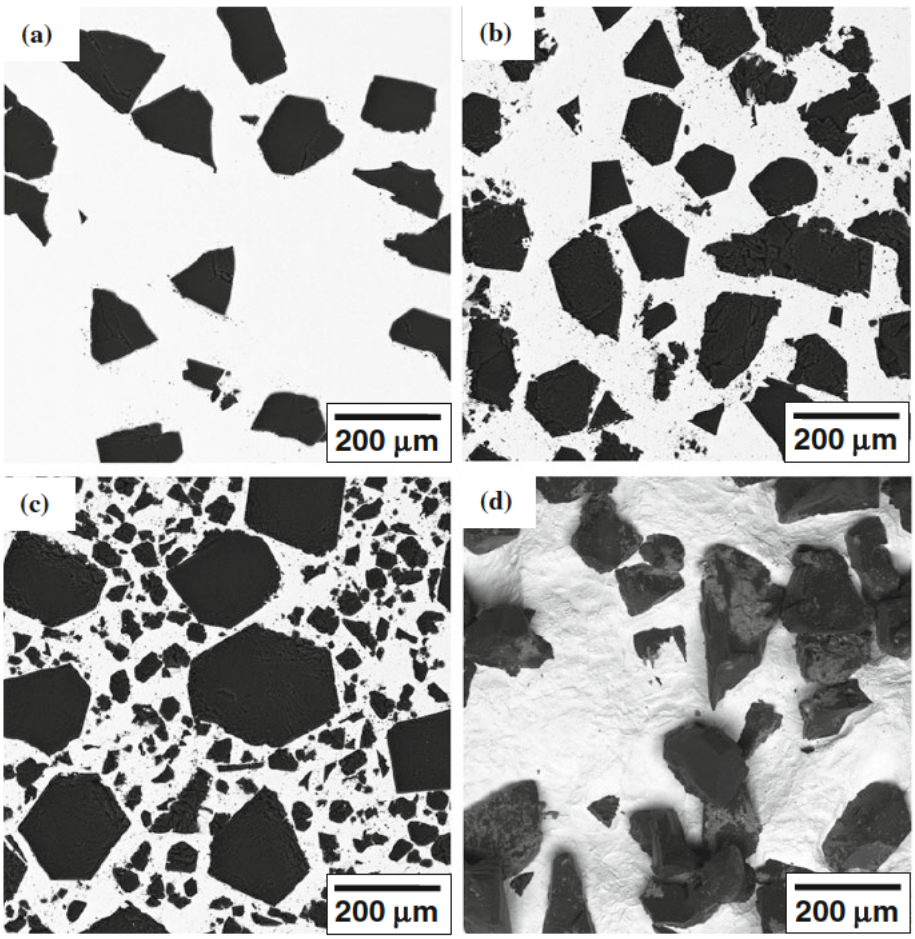

Fig. 1 Microstructure of examined materials: **a** Composite A, **b** Composite B, **c** Composite C, and **d** Composite D. The images were acquired in an SEM with a backscattered electron detector and show the distribution of diamond particles (*dark*) in a copper matrix (*light*)

the morphology, type, and thickness, respectively, of the interfacial carbides. SEM examination was carried out in an FEI Sirion microscope operating at 10 kV using a backscattered electron detector. XRD was carried out using Cu_{K_α} radiation (wavelength = 1.542 Å) in a Rigaku RU200 DMAX B diffractometer operating at 40 kV and 150 mA. The XRD patterns were recorded at the 2θ scan rate of 0.12°/min and step size of 0.008° (θ denotes the Bragg angle). The EPMA experiments were conducted using Cameca SX100 unit operating at 15 or 25 kV. Data from EPMA experiments were modeled to determine the carbide layer thickness. Several software packages (e.g., GMRFILM, Strata and Multifilm) have been developed by different research groups to process the data acquired in an EPMA for determinations of film thickness and composition [21 23]. GMRFILM permits the determination of film thickness (with an accuracy of ±10 %) from experimentally determined X-ray intensity ratios (*k*-ratios) and known film density, as described in Ref. [21]. In the current work, the *k*-ratios for the elements of interest (Cr in the case of particles released from composites A, B, and C; and Si in the case of particles released from composite D) were determined with EPMA experiments using wavelength-dispersive spectrometer (WDS) on the surface carbides (Cr_3C_2 and SiC) on diamond particles extricated from composites and on pure elemental (Cr and Si) standards. The EPMA experiments were conducted at 15 kV on particles extricated from composites A, B, and C, whereas a higher accelerating voltage of 25 kV was needed for multiple locations on particles extricated from composite D. The *k*-ratios and density of carbides ($\rho_{Cr_3C_2} = 6.68 \times 10^3$ kg/m^3 and $\rho_{SiC} = 3.21 \times 10^3$ kg/m^3) were entered in the GMRFILM program to calculate the carbide layer thicknesses, which are shown in Table 3. Prior studies report a good correlation of thin film thickness values determined using EPMA with those determined using Transmission Electron Microscopy [21], Spectroscopic Ellipsometry [21] and Rutherford Backscattering Spectrometry [21, 23]. The experiments in our laboratory on sputter-coated metal films also confirmed a good correlation of thin film thickness values determined using EPMA-GMRFILM method with those determined using Profilometry and Rutherford Backscattering Spectrometry. Therefore, EPMA-GMRFILM technique is expected to provide an accurate value of carbide layer thickness in the current research.

Chemical analysis of extricated particles

The particles extricated from composites A, B, and C (via acid dissolution of Cu-matrix as described above in "Characterization of interfacial carbides" section) were

Distribution Statement A. Approved for public release; distribution unlimited.

Table 3 Carbide layer thickness determined with EPMA GMRFILM technique

Composite	Type of carbide at Cu/diamond interface	Carbide layer thickness[a] (nm)
A	Cr_3C_2	294 ± 136
B	Cr_3C_2	188 ± 67
C	Cr_3C_2	149 ± 46
D	SiC	1255 ± 688

The EPMA experiments were conducted at 15 kV on particles extricated from composites A, B, and C, and at two different accel erating voltages (15 and 25 kV) on particles extricated from com posite D

[a] Mean and standard deviation of thickness values determined at 10 or more different locations are shown

analyzed with Direct Current Plasma Emission Spectroscopy per ASTM E1097 to determine their Cr-content. This analysis facilitates a comparison of the level of Cr-diffusion to the Cu/diamond interface and subsequent interfacial carbide formation in the three composites. This also aids in estimation of the Cr-content of Cu-rich matrix.

Models for thermal properties

Models for interface thermal conductance (h_c)

Three different models for calculation of h_c are considered, and are described below.

Hasselman Johnson/Maxwell Mean-Field (MMF) model

A simple model of the composite is assumed as a distribution of spherical particles (simulating diamond) in a continuous matrix phase (simulating Cu). According to Maxwell theory [24], the effective λ within the framework of such a simple model is given by [25]:

$$\lambda = \lambda_m \left[\frac{2\left(\frac{\lambda_d}{\lambda_m} - 1\right) V_d + \frac{\lambda_d}{\lambda_m} + 2}{\left(1 - \frac{\lambda_d}{\lambda_m}\right) V_d + \frac{\lambda_d}{\lambda_m} + 2} \right], \quad (1)$$

where λ_m is the thermal conductivity of matrix, λ_d is the thermal conductivity of dispersions (i.e., diamond in the current context), and V_d is the volume fraction of dispersions. Equation (1) assumes that there is no interface thermal resistance and therefore, provides the upper-bound for λ. Hasselman and Johnson [26] have proposed a model for λ that incorporates a non-zero interface thermal resistance:

$$\lambda = \lambda_m \left[\frac{2\left(\frac{\lambda_d}{\lambda_m} - \frac{\lambda_d}{a h_c} - 1\right) V_d + \frac{\lambda_d}{\lambda_m} + \frac{2\lambda_d}{a h_c} + 2}{\left(1 - \frac{\lambda_d}{\lambda_m} + \frac{\lambda_d}{a h_c}\right) V_d + \frac{\lambda_d}{\lambda_m} + \frac{2\lambda_d}{a h_c} + 2} \right], \quad (2)$$

where a is the radius of spherical dispersions, and h_c is the interface thermal conductance.

Differential Effective Medium (DEM) scheme

In this model, the composite with a finite volume fraction of dispersions is assumed to be a *homogeneous* material having the same properties as the effective properties of composite [27, 28]. The infinitesimal change in the effective property of composite with an addition of infinitesimal amount of dispersion is given by the dilute solution and this approach leads to a differential equation. Integration of this differential equation, starting at $V_d = 0$ and $\lambda = \lambda_m$, permits an estimation of the effective property (i.e., λ in the current context) of composite at any given V_d within the framework of DEM model. Prior studies report that DEM approach results in a better prediction of composite electrical conductivity than the MMF approach [27, 28]. Moreover, with regards to the predictions of λ, DEM scheme yields consistent results for a wider range of phase contrast (i.e., the ratio of the thermal conductivities of the dispersion and matrix) than the MMF model [29]. Therefore, in addition to the MMF model, DEM approach was considered in the current study, even though the latter is more complex and less commonly used.

The effective thermal conductivity of dispersion is defined as:

$$\lambda_d^{\text{eff}} = \frac{\lambda_d}{\left(1 + \frac{\lambda_d}{a h_c}\right)} \quad (3)$$

Defining conductivity amplification factor, $A = \frac{\lambda}{\lambda_m}$ and the effective phase contrast, $\phi_{\text{eff}} = \frac{\lambda_d^{\text{eff}}}{\lambda_m}$, the governing equation per DEM scheme is [29]:

$$(1 - V_d) = \left(\frac{\phi_{\text{eff}} - A}{\phi_{\text{eff}} - 1}\right) \cdot A^{\ 1/3} \quad (4)$$

Acoustic Mismatch Model (AMM) for h_c calculation

AMM assumes no phonon scattering at the interface [30], and permits an estimation of thermal conductance for Cu/diamond interface without needing the thermal conductivities of the composite and its constituents as the input parameters. According to AMM, the Cu/diamond interface thermal conductance is given by [31, 32]:

$$h_c \approx \frac{1}{2} \rho_m \cdot c_{p_m} \cdot \frac{v_m^3}{v_d^2} \cdot \frac{\rho_m \rho_d v_m v_d}{(\rho_m v_m + \rho_d v_d)^2}, \quad (5)$$

where ρ_m and ρ_d are the densities of Cu and diamond, respectively; v_m and v_d are the phonon velocities in Cu and diamond, respectively; and c_{p_m} is the specific heat capacity of Cu. Using $\rho_m = 8960$ kg/m^3, $c_{p_m} = 385$ J/kg-K, $v_m = 2881$ m/s, $\rho_d = 3520$ kg/m^3 and $v_d = 13924$ m/s as input

Distribution Statement A. Approved for public release; distribution unlimited.

parameters [31] in Eq. (5), h_c for Cu/diamond interface is estimated to be 48.1 × 10^6 W/m^2-K.

Models for CTE

Two models for prediction of composite CTE are considered: the first one was originally proposed by Turner [33] and the second one was originally proposed by Kerner [34]. In the Turner model, a homogeneous strain in the composite is assumed and the shear deformation is assumed to be negligible. By equating the sum of internal forces on any cross-section of the composite to zero, the expression for the composite CTE (α_c) is obtained as [25, 33, 35]:

$$\alpha_c = \frac{\alpha_m V_m K_m + \alpha_d V_d K_d}{V_m K_m + V_d K_d}, \quad (6)$$

where α, V, and K are the CTE, volume fraction, and bulk modulus, respectively, and the subscripts c, m, and d correspond to composite, matrix, and dispersion, respectively. In the Kerner model, the shape of particles is assumed to be spherical and the shear deformation is also considered. This model gives the α_c as [25, 34 36]:

$$\alpha_c = \alpha_m V_m + \alpha_d V_d + V_m V_d(\alpha_d - \alpha_m) \times \frac{K_d - K_m}{V_m K_m + V_d K_d + (3K_m K_d/4G_m)}, \quad (7)$$

where G_m is the shear modulus of matrix. The model predictions of the CTE for Cu diamond composites are obtained with the following matrix and particle properties [25]: $\alpha_{Cu} = 16.42 \times 10^{-6}$/K, $K_{Cu} = 140$ GPa, $G_{Cu} = 49$ GPa, $\alpha_{diamond} = 2.3 \times 10^{-6}$/K and $K_{diamond} = 580$ GPa. The Turner and Kerner model predictions are shown in Fig. 2 as dotted and solid lines, respectively.

Experimental results and model predictions

XRD patterns

The XRD patterns for the diamond particles (along with any interfacial carbide), which were extricated from the four composites, are shown in Fig. 3a d. The pattern from virgin diamond, which has not undergone any consolidation into composite and subsequent acid dissolution of Cu-matrix, is also shown in Fig. 3e for comparison. The diamond peaks are observed from the particles extricated from all the four composites and the Cu-peaks are absent, which suggests a complete dissolution of Cu-matrix. In addition, Cr_3C_2-peaks are also observed from the particles that were extricated from the composites A, B, and C (Fig. 3a c). The number and relative intensities of Cr_3C_2-peaks are the highest for composite A and the lowest for composite C. This suggests that the amount of Cr_3C_2, for a fixed amount of diamond, is the highest on the particles released from composite A, and it is the lowest on the particles released from composite C. For the particles extricated from composite D, XRD pattern shows the SiC peaks (Fig. 3d), in addition to the diamond peaks, and thereby confirms the presence of interfacial SiC.

Morphology of interfacial carbides

The SEM examination of particles extricated from the four composites was carried out and the morphology of interfacial carbides is shown in Fig. 4. In composite A, Cr_3C_2 layer is continuous and covers the interface area almost completely (Fig. 4a). In composite C, Cr_3C_2 layer is discontinuous, and the interface area coverage by Cr_3C_2 is the lowest among composites A, B, and C (Fig. 4). The interface area coverage by Cr_3C_2 in composite B is intermediate between that in composites A and C. In composite D, SiC layer is also discontinuous, and the interface area coverage is even lower than that in composite C by Cr_3C_2 (Fig. 4c d).

Thickness of carbide layers

The thickness of carbide layers is shown in Table 3. The thickness of Cr_3C_2 is the highest in composite A and the lowest in composite C. In conjunction with the carbide morphology described above, this indicates that the more continuous a Cr_3C_2 layer is, the thicker it is. This further

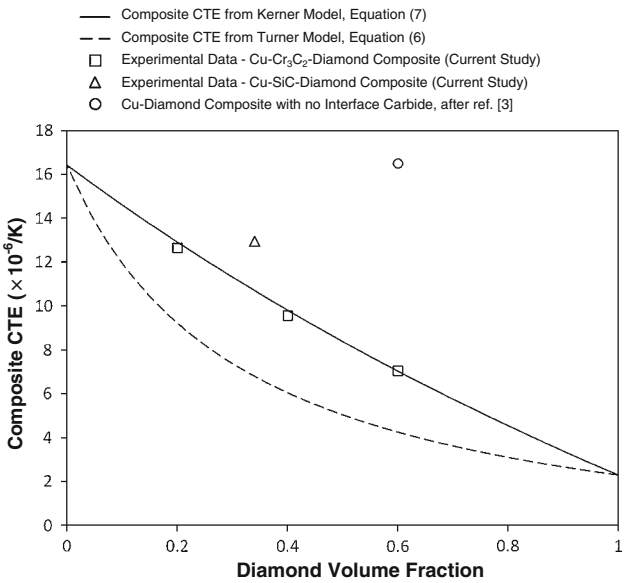

Fig. 2 Comparison of experimentally measured CTE of composites A, B, C, and D with the predictions of Turner and Kerner Models. The CTE of Cu diamond composite with no interface carbide, taken from Ref. [3], is also shown

Distribution Statement A. Approved for public release; distribution unlimited.

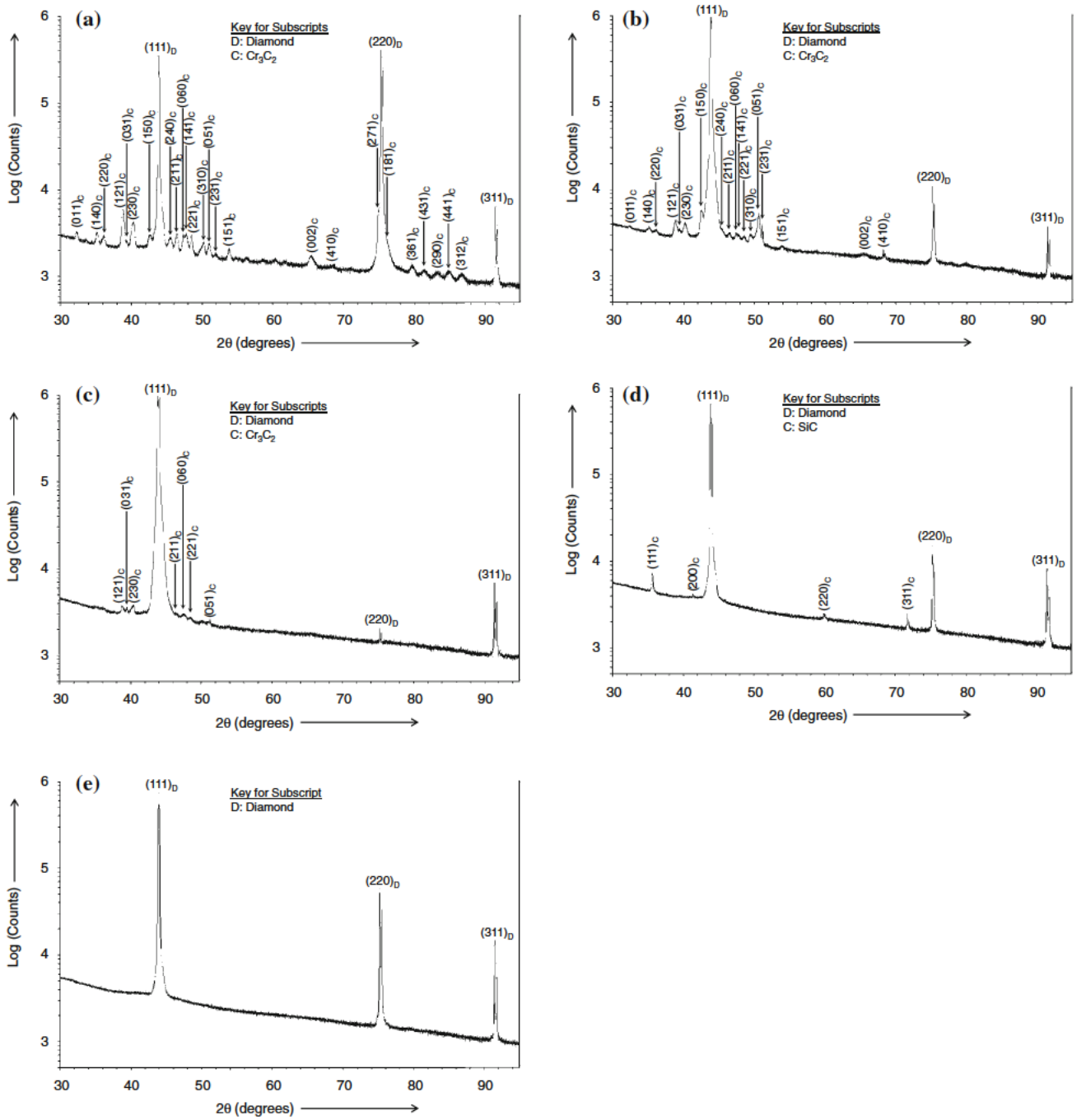

Fig. 3 XRD patterns of particles extricated from: **a** Composite A, **b** Composite B, **c** Composite C, and **d** Composite D. **e** shows the XRD pattern for virgin diamond particles that had not undergone any consolidation into composite and subsequent acid dissolution of Cu matrix. The XRD peaks were identified with Powder Diffraction File (PDF) of the International Centre for Diffraction Data. The peaks identified as diamond, Cr_3C_2 and SiC match the best with PDF# 06 0675 (Diamond), 35 0804 (Tongbaite) and 29 1129 (Moissanite 3C), respectively. Tongbaite (crystal structure: primitive orthorhom bic) and Moissanite 3C (crystal structure: face centered cubic) are minerals with chemical formulae Cr_3C_2 and SiC, respectively

suggests that the amount of Cr_3C_2 is not fixed for a given diamond particle size and it varies with the diamond vol% of the composite. A higher amount of Cr_3C_2 (for a given interfacial area) is associated with a lower vol% of diamond in the composite and this finding is consistent with the XRD results. The thickness of interfacial SiC in composite D is significantly higher than that of Cr_3C_2 in even composite A (Table 3).

Distribution Statement A. Approved for public release; distribution unlimited.

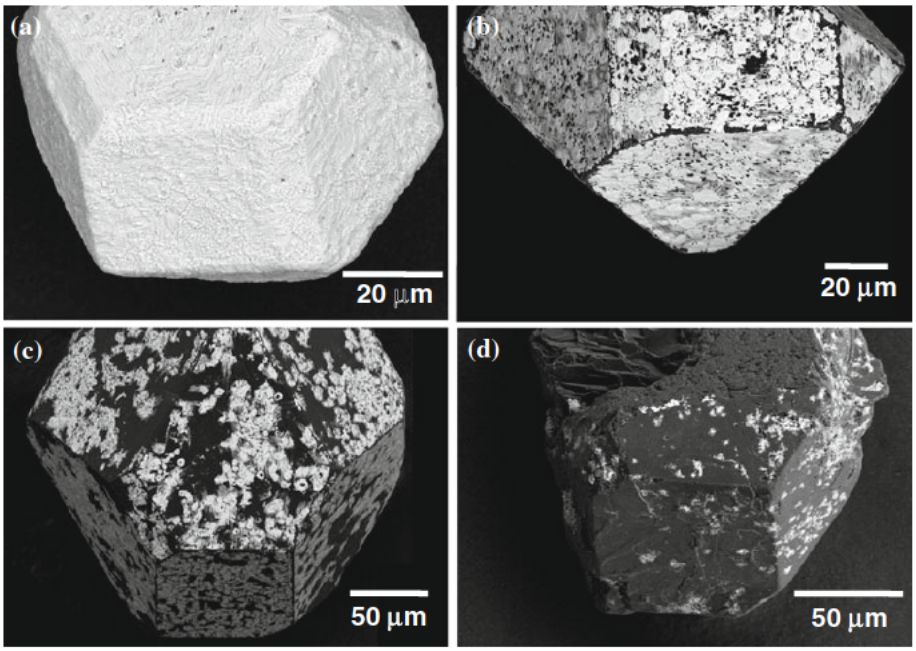

Fig. 4 Backscattered electron (BSE) images of diamond particles, along with interfacial carbides, extricated from the four Cu diamond composites examined in this study. The morphology of interfacial carbides (*bright regions*) on diamond (*dark regions*) is shown for: **a** Composite A, **b** Composite B, **c** Composite C, and **d** Composite D

Table 4 Cr content and amount of Cr_3C_2 in powders extricated from the three Cu Cr_3C_2 diamond composites

Examined material	Cr content of extricated powders[a] (wt%)	Amount of Cr_3C_2 in extricated powders		Cr content of Cu rich matrix (wt%)[d]
		(wt%)[b]	(vol%)[c]	
Composite A	5.43	6.27	3.40	0.23
Composite B	1.72	1.98	1.06	0.34
Composite C	0.54	0.62	0.33	0.48

Cr content of Cu rich matrix is also shown

[a] The Cr content of extricated powders was determined with Direct Current Plasma Emission Spectroscopy per ASTM E1097 07

[b] Equation used to obtain this set of data: Amount of Cr_3C_2 in extricated powders (wt%) $\left(\frac{180}{156}\right) \times$ (Cr content of extricated powders in wt%). The numerator of 180 in this equation is the molecular weight of Cr_3C_2, and the denominator of 156 is 3× the atomic weight of Cr

[c] This set of data was calculated from the amount of Cr_3C_2 in extricated powders in wt%, and with densities of Cr_3C_2 and dia mond 6.68×10^3 and 3.52×10^3 kg/m^3, respectively

[d] This set of data was calculated from the difference of Cr amount added initially as Cu 0.8Cr alloy and amount of Cr involved in formation of interfacial Cr_3C_2

Chemistry of extricated particles

The Cr-content of powders extricated from composites A, B, and C is shown in Table 4. The amount of Cr_3C_2 in extricated powders was calculated from their respective Cr-contents and is also shown in Table 4. The amount of Cr_3C_2 in powder extricated from composite A is an order of magnitude higher than that from composite C. The amount of Cr_3C_2 in powder extricated from composite B is intermediate between that from composites A and C. This finding is consistent with the results presented above in "XRD patterns", "Morphology of interfacial carbides", and "Thickness of carbide layers" sections. Moreover, Cr-content of Cu-rich matrix is the lowest in composite A and the highest in composite C (Table 4). The reason for this trend in matrix Cr-content with a change of diamond vol% is currently unclear.

Thermal properties

The Maxwell theory predicted and experimentally determined values of λ for the four composites are shown in Table 5. The mismatch between the two set of values suggests that the interface thermal resistance plays an important role in affecting λ. The h_c values were computed using Hasselman Johnson model (Eq. (2)) as well as DEM model (Eqs. (3 4)), and are also presented in Table 5. The two models provide similar estimates of h_c. As expected, λ increases with an increase of diamond vol% for the three Cu Cr_3C_2 diamond composites (A, B, and C). There are

Distribution Statement A. Approved for public release; distribution unlimited.

Table 5 Experimentally measured values of Coefficient of Thermal Expansion (CTE) and thermal conductivity for the four copper diamond composites

Composite	Amount of diamond (vol%)	Nitrogen content of diamond used[a] (ppm)	Thermal conductivity of diamond used[b] (W/m K)	Composite thermal conductivity predicted with Maxwell theory[c], Eq. (1) (W/m K)	Experimentally determined		Average diamond particle radius, a (μm)	h_c from H J model[c], Eq. (2) ($\times 10^6$ W/m^2 K)	DEM model Results[c]	
					Composite CTE ($\times 10^{-6}$/K)	Composite thermal conductivity (W/m K)			h_c from Eqs. (3 4) ($\times 10^6$ W/m^2 K)	Effective phase contrast, ϕ_{eff}
A	20	180	1623	535	12.66	478	55	39.3	38.3	2.3
B	40	180	1623	704	9.57	591	55	50.9	47.8	2.5
C	60	238	1429	860	7.06	601	78	21.8	21.5	1.9
D	34	59	2013	691	12.96	270	55	1.6	1.7	0.2

The predicted thermal conductivity of composite using Maxwell theory and the calculated thermal conductance (h_c) values for the Cu/diamond interface using two different models are also shown

[a] The nitrogen content of diamond was determined with inert gas fusion method

[b] The diamond thermal conductivity was estimated from its nitrogen content, using the results reported in Ref. [37]

[c] A matrix thermal conductivity of 400 W/m K was assumed for all the four composites

four independent factors that determine the effective λ: (i) volume fraction of constituents, (ii) thermal conductivity of constituents, (iii) size of diamond particles, and (iv) thermal conductance across the metal/diamond interface. A consideration of h_c values for the different composites permits a relative assessment of the efficacy of the interface with regards to the thermal transport between Cu and diamond, which is not possible from a consideration of λ values alone. Among the three Cu Cr_3C_2 diamond composites, composite B has the highest h_c and composite C has the lowest h_c. This implies that the thermal transport across Cu/diamond interface is the most efficient in composite B and the least efficient in composite C, although composite C has the highest λ (Table 5). Composite D (i.e., the Cu SiC diamond composite) has a lower h_c than even composite C. However, composite D has a higher h_c than a value of 0.5×10^6 W/m^2-K, which has been reported in an earlier study for Cu diamond composite with no interfacial carbides [6]. This suggests that even in the composite with the lowest h_c in the current study, the heat transfer across Cu/diamond interface is more efficient than in a Cu diamond composite with no interfacial carbides. The ϕ_{eff} of the four composites examined in this study has values in the range of 0.2 2.5 (Table 5). The good agreement between the MMF and DEM predictions of h_c in this range of ϕ_{eff} is consistent with an earlier study [29] that reported a significant disagreement between the predictions of two models at $\phi_{eff} > 4$ and a good agreement at $\phi_{eff} = 2 - 4$.

The experimentally determined values of CTE for the four composites are also shown in Table 5. As expected, a lower CTE is associated with a higher diamond vol% in the three Cu Cr_3C_2 diamond composites (A, B, and C). The experimental data are compared with the Turner and Kerner model predictions in Fig. 2. The previously reported [3] CTE for a Cu diamond composite with no interfacial carbide is also shown in Fig. 2. The three Cu Cr_3C_2 diamond composites follow the Kerner line and this suggests that shear deformation does occur with a change of temperature in these composites. Unlike h_c, the degree of agreement of CTE with the model prediction does not depend on the Cr_3C_2 layer thickness and continuity, within the range examined in this study. On the other hand, the CTE of composite D is higher than both the Turner and Kerner model predictions. This suggests a weaker bonding between Cu and diamond in composite D than in composites A, B, and C. This effect could possibly be associated with the differences in type, morphology and/or thickness of the interfacial carbides in the two types of composites (i.e., Cu Cr_3C_2 diamond and Cu SiC diamond). However, the degree of disagreement from model predictions of CTE for Cu diamond composite (with no interfacial carbide) is even higher than for composite D, suggesting a stronger bonding between Cu and diamond in the latter composite. This trend in CTE values for the three different types of composites (i.e., Cu Cr_3C_2 diamond, Cu SiC diamond, and Cu diamond with no interfacial carbide) is consistent with the trends in λ and h_c values for these three types of materials, as described above. In general, a lower CTE is associated with a higher λ and a higher h_c, which is in agreement with prior studies. For example, Weber and Tavangar have reported a higher λ

Distribution Statement A. Approved for public release; distribution unlimited.

and a lower CTE for Cu B_4C diamond composites than for Cu Cr_3C_2 diamond composites [3].

Discussion

A new finding of this study is that in Cu diamond composites, which are fabricated using pre-alloyed Cu 0.8Cr powder, the interfacial carbide layer thickness and continuity vary significantly with a change of diamond vol%. A thicker and more continuous Cr_3C_2 layer is associated with a lower diamond vol%. This variation is caused by three factors: (i) for a fixed quantity of composite, a higher amount of Cr is present in the lower diamond vol% composite; (ii) a higher fraction of available Cr participates in the formation of interfacial Cr_3C_2 in the lower diamond vol% composite, as suggested by the Cr-content of matrix in composites A, B and C (Table 4); and (iii) for a given quantity of composite, the total Cu/diamond interface area is smaller for the lower diamond vol% composite. This finding has important implications for improving our understanding of the factors that affect thermal transport across Cu/diamond interfaces and overall thermal conductivity of Cu diamond composites. In prior studies [4 6], the importance of interfacial carbide layer thickness in affecting h_c is discussed. However, earlier investigations have reported a continuous carbide layer at Cu/diamond interfaces based on characterization of sections through small areas [4, 5], and characterizations in this study of significantly larger interfacial areas indicate that this clearly is not the case for all material/processing conditions. A comparison of h_c values for composites A and B (Table 5) shows that a more continuous interfacial carbide layer does not necessarily lead to an improved interfacial thermal conductance if this higher level of continuity is associated with an increase in carbide layer thickness. This is, at least in part, due to thermal conductivity of Cr_3C_2 (Table 1) being significantly lower than that of both Cu and diamond. On the other hand, a comparison of h_c values for composites B and C (Table 5) demonstrates that a thinner interfacial carbide layer also does not necessarily lead to an improved interfacial thermal conductance if this reduction in thickness is associated with a reduction in continuity of the carbide layer. Moreover, there is a good agreement of h_c for composite B with the AMM prediction (See "Acoustic Mismatch Model (AMM) for h_c calculation" section). Based on the experimental evidence and model estimates presented in this study, we propose that the maximum possible h_c value will be attained for the condition of a *thin and continuous* interfacial carbide layer. The attainment of the highest possible h_c has practical importance as it would lead to a composite with the highest possible λ at a given particle size and volume fraction of diamond. For example, a composite with the diamond particle size, volume fraction and nitrogen content as in composite C, and an $h_c = 50.9 \times 10^6$ W/m^2-K as in composite B, is predicted to have a $\lambda = 721$ W/m-K from MMF model (Eq. (2)). This is 20 % higher than the λ of composite C (Table 5) and is, in principle, attainable by changing the interfacial Cr_3C_2 layer characteristics.

In an earlier study [3], for a given diamond particle size and volume fraction, the λ was reported to first increase with Cr-content of the starting Cu Cr alloy, reach a maximum at Cr-content $\sim$0.5 at% (i.e., $\sim$0.4 wt%) and then decrease at Cr-content >0.4 wt%. The decrease of λ at Cr-content >0.4 wt% was suggested to be due to the possibility of a reduction in matrix thermal conductivity as a result of any residual Cr as solid solution in the Cu-rich matrix [3]. However, the results of current study suggest that any possible variation in the characteristics of interfacial carbide layer (e.g., higher thickness with similar continuity at Cr-content >0.4 wt%) can also reduce h_c and thereby, the λ. This could be an alternate mechanism that can explain the lower λ at Cr-content >0.4 wt% reported in Ref. [3]. To determine the relative contributions of two mechanisms (i.e., a reduced matrix thermal conductivity and a reduced h_c), additional data from composites in Ref. [3] may be needed.

The Cu SiC diamond composite has substantially lower λ and an order of magnitude lower h_c than the Cu Cr_3C_2 diamond composites examined in this study (Table 5). Figure 4 shows that the interfacial carbide is less continuous and sparser in composite D than in composites A, B, or C. In this regard, it is also important to note that the Cu SiC diamond composite has a higher λ and a higher h_c than the values reported in prior studies [3, 6] for Cu diamond composites with no interfacial carbide layer. Weber and Tavangar [3] reported a $\lambda \sim 130$ W/m-K for a Cu 60 vol% diamond composite with no interfacial carbide and an average diamond particle diameter of $\sim$200 μm. Schubert et al. [6] reported a $\lambda = 215$ W/m-K and an $h_c = 0.5 \times 10^6$ W/m^2-K, for a Cu 42 vol% diamond composite with no interfacial carbide and an average diamond particle diameter of 120 μm. Therefore, the presence of SiC at the Cu/diamond interface does lead to an improvement in thermal transport between Cu and diamond. A lower λ and h_c in composite D than in composites A, B or C can, at least in part, be attributed to the differences in the interfacial carbide layer morphology and thickness. To determine the degree of dependence of h_c on the type of interfacial carbide (i.e., SiC vs. Cr_3C_2), an examination of Cu SiC diamond composites with a significantly ($\sim$ an order of magnitude) thinner and more continuous interfacial SiC layer than in composite D is needed.

The degree of agreement of the CTE with the Kerner model prediction is same for the three Cu Cr_3C_2 diamond

Distribution Statement A. Approved for public release; distribution unlimited.

composites (A, B and C) examined in this study. On the other hand, the degree of agreement of h_c with the AMM prediction is different for the composites A, B, and C. The continuity and thickness of interfacial Cr_3C_2 layer are also different for these three composites. These results indicate that within the range of interfacial carbides examined in this study, the thickness and continuity of Cr_3C_2 has a strong influence on the h_c but not on the CTE. This finding is consistent with a previous study [3], where a constant CTE and variations in λ at Cr-content in the range 0.1 1 at% (i.e., 0.08 0.82 wt%) were reported for a fixed volume fraction and particle size of diamond. The variations in λ at Cr-content of 0.1 1 at% reported in Ref. [3] could possibly be associated with the variations in h_c, as discussed in the current paper.

Summary and conclusions

The thermal properties of Cu diamond composites with two different types of interfacial carbides, Cr_3C_2 and SiC, were examined. A higher processing temperature and time were employed to fabricate the Cu Cr_3C_2 diamond composites than the Cu SiC diamond composite. A higher processing temperature/time combination for Cu Cr_3C_2 diamond composites facilitates Cr-diffusion to the metal/diamond interface with the resultant formation of interfacial Cr_3C_2, whereas a lower temperature/time combination for Cu SiC diamond composite limits the decomposition of SiC already present at the Cu/diamond interface and any subsequent diffusion of Si into the Cu-matrix. The conclusions of this study are summarized below:

(i) In the Cu Cr_3C_2 diamond composites, the morphology and thickness of interfacial Cr_3C_2 layer are not fixed, but vary with the volume fraction and particle size of diamond. For a lower Cu/diamond interfacial area per unit volume of the composite, the Cr_3C_2 layer is thicker and more continuous.

(ii) In the examined Cu SiC diamond composite, the interfacial SiC is not continuous, but sparse. The h_c and λ values for Cu SiC diamond composite are lower than those for Cu Cr_3C_2 diamond composites, but are higher than those reported in prior studies for Cu diamond composites with no interfacial carbides.

(iii) The h_c and λ values are strongly dependent on the interfacial carbide layer morphology and thickness. A thin and continuous carbide layer is likely to result in the highest possible heat transfer between Cu and diamond, and thereby a maximum possible λ for a given diamond particle size and volume fraction.

(iv) To determine the relative efficacy of the two carbides, Cr_3C_2 and SiC, for improving the thermal conductance between Cu and diamond, additional research on Cu SiC diamond composites with a different SiC layer morphology and thickness is needed.

(v) This study suggests an alternative mechanism for a previously reported lower λ at Cr-content >0.4 wt%, which is based on the expected changes in h_c, attributable to the possible variations in interfacial Cr_3C_2 layer thickness with an increase in Cr-content. This alternate mechanism is different from the mechanism of reduced matrix thermal conductivity, attributable to a possible higher amount of Cr as solid solution in the matrix at the higher Cr-content, which was proposed in an earlier study.

(vi) The CTE of Cu Cr_3C_2 diamond composites with 20 60 vol% diamond matches well with the Kerner model predictions and not with the Turner model predictions. This suggests deformation involving shear during temperature excursions of these composites.

(vii) The CTE of Cu SiC diamond composite is higher than that predicted by the Turner and Kerner models. However, the degree of agreement with models is better for Cu SiC diamond composite than for a Cu diamond composite with no interfacial carbide. This suggests that within the range of interfacial carbide type, thickness, and morphology examined in this study, the bonding between Cu and diamond is stronger in Cu Cr_3C_2 diamond composites than in the Cu SiC diamond composite. Moreover, this bonding is stronger in Cu SiC diamond composite than in the Cu diamond composite with no interfacial carbides.

(viii) Composite CTE is inversely related to its λ and h_c. Therefore, it can serve as a quick, effective, and relative measure of the state of Cu/diamond interface in the context of thermal transport, under the conditions of a fixed diamond size and volume fraction.

Acknowledgements This research was supported by Air Force Office of Scientific Research under Thermal Sciences Portfolio (Program Manager: Dr. Joan Fuller, LRIR # 11RX02COR) and per formed at Air Force Research Laboratory, Materials and Manufac turing Directorate (Contract # F33615 04 D 5235 and FA8650 10 D 5226). The authors thank Dr. S. Ganguli (UDRI) and Dr. A. Roy (AFRL) for help in initiating thermal property measurements. Dr. F. Meisenkothen (UES, Inc.) and Mr. Jared Shank (UES, Inc.) helped with the carbide layer thickness measurements via EPMA GMRFILM Model. Drs. C. Muratore and B.M. Howe (both at AFRL) helped with the Profilometry and Rutherford Backscattering Spec trometry experiments to determine the thickness of metal thin films. We acknowledge the assistance of Mr. Bob Lewis (UES, Inc.) with acid dissolution experiments and with specimen preparation for microstructural examination. Thanks to Mr. Henry "Mic" Meeks of AM^2T, LLC (formerly Ceracon, Inc.) for providing consolidated Cu SiC diamond composite, and to Dr. Thomas Schubert (IFAM, Dresden, Germany) for providing virgin diamond particles for nitro gen analysis.

Distribution Statement A. Approved for public release; distribution unlimited.

References

1. Zweben C (2004) In: Zediker MS (ed) High power diode laser technology and applications II, Proc SPIE, vol 5336, Bellingham, WA, pp 166 175
2. Ludtke A, Leichtfried G (2006) Patent No. US 0157884 Al
3. Weber L, Tavangar R (2007) Scr Mater 57:988
4. Schubert T, Ciupiński Ł, Zieliński W, Michalski A, Weißgärber T, Kieback B (2008) Scr Mater 58:263
5. Schubert T, Weißgärber T, Kieback B (2009) Adv Mater Res 59:169
6. Schubert T, Trindade B, Weißgärber T, Kieback B (2008) Mater Sci Eng A 475:39
7. Pierson HO (1996) Handbook of refractory carbides and nitrides: properties, characteristics, processing and applications. Noyes Publications, Westwood, p 146
8. Ault NN (2001) In: Buschow KHJ, Cahn RW, Flemings MC, Ilschner B, Kramer EJ, Mahajan S (eds) Encyclopedia of mate rials science and technology, vol 9. Elsevier Science Ltd., Oxford, pp 8506 8507
9. Neudeck PG (2001) In: Buschow KHJ, Cahn RW, Flemings MC, Ilschner B, Kramer EJ, Mahajan S (eds) Encyclopedia of mate rials science and technology, vol 9. Elsevier Science Ltd., Oxford, p 8509
10. Harris GL (1995) Properties of silicon carbide, INSPEC. The Institution of Electrical Engineers, London, p 5
11. Pierson HO (1996) Handbook of refractory carbides and nitrides: properties, characteristics, processing and applications. Noyes Publications, Westwood, p 148
12. Pierson HO (1996) Handbook of refractory carbides and nitrides: properties, characteristics, processing and applications. Noyes Publications, Westwood, p 103
13. Yang X, Yue Qing S, Chen Guang L, Shun C, Zhen Zheng F (2009) Trans Nonferrous Met Soc China 19:1161
14. Sundberg G, Paul P, Sung C, Vasilos T (2004) Adv Microelectron 31(6):8
15. Sundberg G, Paul P, Sung C, Vasilos T (2005) J Mater Sci 40:3383. doi:10.1007/s10853 005 2847 1
16. Sundberg G, Paul P, Sung C, Vasilos T (2006) J Mater Sci 41:485. doi:10.1007/s10853 005 2622 3
17. Pickard SM, Withers JC, Loutfy RO (2007) Patent No. US 7279023 B2
18. Spowart JE, Maruyama B, Miracle DB (2008) Patent No. US 7364692 B1
19. Lide DR (2009) CRC handbook of chemistry and physics, 90th edn. Taylor & Francis Group, Boca Raton, p 4 135
20. Barin I (1995) Thermochemical data of pure substances, vol 1, 3rd edn. VCH, Weinheim, p 211
21. Waldo RA, Militello MC, Gaarenstroom SW (1993) Surf Inter face Anal 20:111
22. Pouchou JL, Pichoir F (1993) Scanning Microsc Suppl 7:167
23. Pouchou JL (1993) Anal Chim Acta 283:81
24. Maxwell JC (1946) A treatise on electricity and magnetism, vol I, 3rd edn. Oxford University Press, London, p 440
25. Yoshida K, Morigami H (2004) Microelectron Reliab 44:303
26. Hasselman DPH, Johnson LF (1987) J Compos Mater 21(6):508
27. Weber L, Fischer C, Mortensen A (2003) Acta Mater 51:495
28. Weber L, Dorn J, Mortensen A (2003) Acta Mater 51:3199
29. Tavangar R, Molina JM, Weber L (2007) Scr Mater 56:357
30. Swartz ET, Pohl RO (1989) Rev Mod Phys 61(3):605
31. Chu K, Liu Z, Jia C, Chen H, Liang X, Gao W, Tian W, Guo H (2010) J Alloy Compd 490:453
32. Chu K, Jia C, Liang X, Chen H, Gao W, Guo H (2009) Mater Des 30:4311
33. Turner PS (1946) J Res Natl Bur Stand 37:239
34. Kerner EH (1956) Proc Phys Soc B 69:808
35. Lemieux S, Elomari S, Nemes JA, Skibo MD (1998) J Mater Sci 33:4381. doi:10.1023/A:1004437032224
36. Hsieh CL, Tuan WH (2007) Mater Sci Eng A 460 461:453
37. Yamamoto Y, Imai Y, Tanabe K, Tsuno T, Kumazawa Y, Fuji mori N (1997) Diam Relat Mater 6:1057

Distribution Statement A. Approved for public release; distribution unlimited.